PAVEMENT STRUCTURAL ASSESSMENT USING FINITE ELEMENT MODELING AND MECHANISTIC GEOTECHNICAL TOOLS

Prepared by:

Curtis Berthelot, Roberto Soares, Duane Guenther,

Rielle Haichert, Diana Podborochynski, Brent Marjerison

Paper prepared for presentation at the

Sessions: Innovation in Geotechnical and Materials Engineering

2016 Annual Conference of the Transportation Association of Canada

Toronto, ON

ABSTRACT

In road construction, the *in situ* material properties, roadway design and construction practices all have impact on its final quality and its life cycle performance. To better understand performance risk of roadways, numerical modeling of pavements can be used. This paper presents the results of a project that involved taking borehole core samples of the as-built roadway and conducting a full suite of geotechnical and mechanistic tests on the *in situ* materials. The material constitutive properties were then used as inputs into a finite element model to provide structural responses and therefore insight into the expected road performance.

This paper summarizes the findings where potential performance issues are expected due to variable *in situ* conditions as identified during construction. The *in situ* road condition was modelled based on the material properties characterized and theoretical field state condition scenarios specific to this roadway. The finite element model characterized the effect of the *in situ* variability under typical truck loading specified for the road as well as climatic conditions typical of the area. The results of the modelling investigation showed significant variation in structural primary responses. Based on the primary response profiles of the various road segments modelled under realistic Canadian field state conditions, the *in situ* variability is expected to have highly variable life cycle structural performance.

INTRODUCTION

In road construction, the *in situ* material properties, roadway design and construction practices all have impact on a road's final quality and its life cycle performance. In order to understand risk and responsibility in the case of roadway performance, agencies can use finite element modeling as a roadway design tool. Roadway design using finite element modeling involves taking borehole core samples of the as-built roadway and conducting a full suite of geotechnical and mechanistic tests on the material. The material constitutive properties can then be input into a finite element model to provide insight into the expected road performance. This paper details the investigation results from the geotechnical testing, mechanistic testing, and finite element modeling of a heavy haul roadway in Western Canada.

The objectives of this project were twofold. First, to conduct laboratory characterization of soil samples. Secondly, to perform structural finite element modeling of the roadway segments. Part of the objective was also to segment the road based on material classification and *in situ* properties, and to perform mechanistic characterization and structural modeling of the control section segments, across theoretical optimum moisture content and density as well as the range of field measured moisture-density conditions.

Once the mechanistic testing was complete, finite element modeling using field state material properties was conducted to determine the response of baseline road case using the available materials and good construction practices (optimum conditions) and to compare this to the measured conditions encountered on the control section.

Mechanistic Numerical Analysis

Conventional road design has been utilizing empirical methods or a combination of mechanistic-empirical methodologies that typically employ inelastic orthogonal strains to make calculations and predict field performance (1,2). Roadway analysis and design has been benefiting from 3D finite element road modeling techniques and non-linear inelastic material constitutive theory (3). In particular, accurate shear strains are highly correlated to performance and failure criterion of a road structure and provide more accurate predictions than simply orthogonal strains. Shear strain predictions provide realistic correlation with unusual and hard-to-predict scenarios, such as off-ramps, slow moving traffic lanes, bus stops and others.

Advanced mechanistic materials characterization and numerical modeling were performed on a roadway for this paper, similar methods have been used previously (4,5). The road model used in this study has been validated by comparing model-generated peak deflections to field-measured peak deflections using non-destructive failing weight deflectometer (FWD) testing. A study was conducted to validate the structural road modeling deflection response by field falling weight deflectometer testing (6). A finite element numerical model, coupled with roadway extracted samples, was used to make performance predictions of a haul road structure under various stress states. Material properties such as Poisson's ratio and dynamic modulus were obtained from various mechanistic laboratory tests and used as inputs into the finite element model. The model was then able to predict a deflection response based on a simulated truck load as well as strains and stresses in the pavement structure based on a set of different loads and geometries (7,8,9). The Unified Soil Classification System (USCS) characterization across the road segments was used to distinguish between subgrade types. *In situ* moisture content and density was measured and compared to proctor optimum for each road segment to determine range in the as-built conditions. Figure 1 below displays an example of the PSIPave3D^{TM} Model set-up.

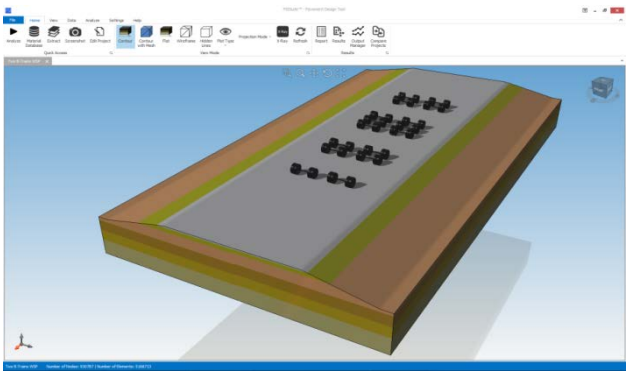

Figure 1 Examples of PSIPave3D™ Model Set-Up

PROJECT METHODOLOGY

The design methodology for this study was split in three steps: geotechnical material characterization (step 1), non-linear mechanistic material characterization (step 2), and finite element modeling (step 3). Two roadway segments were analyzed: km 1.40 to 2.11 and km 2.11 to 4.90. There were two borrow pits used for the construction of the roadway: borrow pit (BP) A and BP B. The subgrade materials for the first segment, from km 1.40 to 2.11, were taken from BP A. The subgrade materials for the second segment, from km 2.11 to 4.90, were taken from borrow pit BP B.

As part of the geotechnical material characterization (step 1), samples collected from the control section included both disturbed samples as well as Shelby tube samples. As part of the laboratory testing program, preliminary laboratory characterization of the subgrade soils was completed and the *in situ* moisture-density properties of the subgrade soils were compared to the optimum moisture density of each borrow pit subgrade soil. Laboratory characterization of the granular base materials was also completed.

Preliminary laboratory characterization was performed on the targeted *in situ* subgrade material samples and included grain size distribution (ASTM D6913), unified soil classification system (USCS) (ASTM D2487), Atterberg limits characterization (ASTM D3282), *in situ* moisture and density characterization (ASTM C566 and D698) and unconfined compressive strength and stiffness (UCCS) (ASTM D2166).

As part of the non-linear mechanistic material characterization (step 2), mechanistic testing using non-linear rapid triaxial frequency sweep characterization was conducted on the subgrade soil from BP A and BP B, as well as the granular base used on the project.

As part of the finite element modeling (step 3), the finite element modeling used a standard B-Train truck load on a 50 m long pavement, two-lane pavement mesh with over 5 million elements. Non-linear stress dependent materials properties obtained from the laboratory were used as inputs. Pavement lanes are 3.7m wide, shoulders are 3 m wide with a 5:1 side slope. A B-Train load (8 axles and 62,500kg total) was applied to the pavement. The driving lane layer pavement thicknesses are 120 mm hot mix asphalt concrete (HMAC) and 400mm base and the passing lane thicknesses are 100 mm HMAC and 350 mm base.

LABORATORY GEOTECHNICAL CHARACTERIZATION RESULTS

As shown in Table 1, the USCS soil fines classification of the subgrade in BP A ranged from low plastic clay (CL) to intermediate plastic clay (CI). The USCS soil fines classification of the subgrade in borrow pit (BP) B ranged from low plastic clay (CL) to intermediate plastic clay (CI) with localized areas of plastic silt (ML).

Table 1 PI and USCS Soil Classification Results

Test Holes	Borrow Pit (BP)	Location (km limits)	Subgrade Type	Sample Quantity	Plastic Index			Plastic Index Coefficient of Variance	USCS
					Avg	Min	Max		
1 to 8	BP A	1.40 to 2.11	Side Slopes	9	21	10	26	**20.1%**	CL,CI
			Road Core	6	20	16	24		CL,CI
			Deep *in situ*	3	22	21	23	**5.3%**	CI
9 to 14	BP B	2.11 to 4.90	Side Slopes	23	18	15	27	**17.1%**	CL,CI
			Road Core	9	14	0	24		ML,CL,CI
			Deep *in situ*	5	18	15	19	**10.7%**	CL

Given the relatively high variability observed from the *in situ* subgrade moisture and density Shelby samples, an evaluation of all *in situ* subgrade moisture contents from both Shelby and auger samples was performed. As seen in Table 2, Figure 2 and Figure 3, the *in situ* subgrade moisture of the road ranged from -14.0% to 8.4% difference from standard optimum moisture content from km 1.40 to km 2.11. From km 2.11 to km 4.9, the *in situ* subgrade moisture of the main road ranged from -4.7% to 12.5%. It can be seen from Figure 2 and Figure 3 that the moisture and density of the *in situ* subgrade samples provided were variable relative to standard Proctor optimum across all of the borrow pits, meaning the subgrade moisture was highly variable on this roadway.

Table 2 *In situ* Moisture Relative to Standard Proctor Optimum

Test Holes	Borrow Pit (BP)	Location (km limits)	Subgrade Type	Sample Quantity	Difference from Optimum Moisture Content			Range in Difference from Opt. Moisture
					Avg	Min	Max	
1 to 8	BP A	1.40 to 2.11	Side Slopes	14	1.5%	-11.4%	8.3%	**-14.0% to 8.4%**
			Road Core	7	-4.6%	-14.0%	0.9%	
			Deep *in situ*	8	2.3%	-3.0%	8.4%	
9 to 14	BP B	2.11 to 4.90	Side Slopes	31	3.0%	-1.5%	12.5%	**-4.7% to 12.5%**
			Road Core	9	-2.4%	-4.7%	-0.3%	
			Deep *in situ*	18	2.8%	-0.8%	11.7%	

Table 3 details the *in situ* subgrade dry density of each test hole and borrow pit relative to standard Proctor optimum dry density. As seen in Table 3, Figure 2 and Figure 3, the *in situ* subgrade dry density of the main road ranged from 97% to 102% from km 1.40 to km 4.90. The dry density of the subgrade from km 1.40 to km 4.90 was also variable.

Table 3 ***In situ*** **Shelby Dry Density Relative to Standard Proctor Optimum**

Test Holes	Borrow Pit (BP)	Location (km limits)	Subgrade Type	Sample Quantity	Percent of Optimum Dry Density			Range in % of Opt. Density
					Avg	Min	Max	
Main Road								
1 to 8	BP A	1.4 to 2.11	Side Slopes	5	101%	100%	102%	**97% to 102%**
			Road Core	4	98%	97%	100%	
			Deep *in situ*	0	--	--	--	
9 to 14	BP B	2.11 to 4.9	Side Slopes	6	96%	85%	102%	**85% to 102%**
			Road Core	3	98%	96%	101%	
			Deep *in situ*	0	--	--	--	

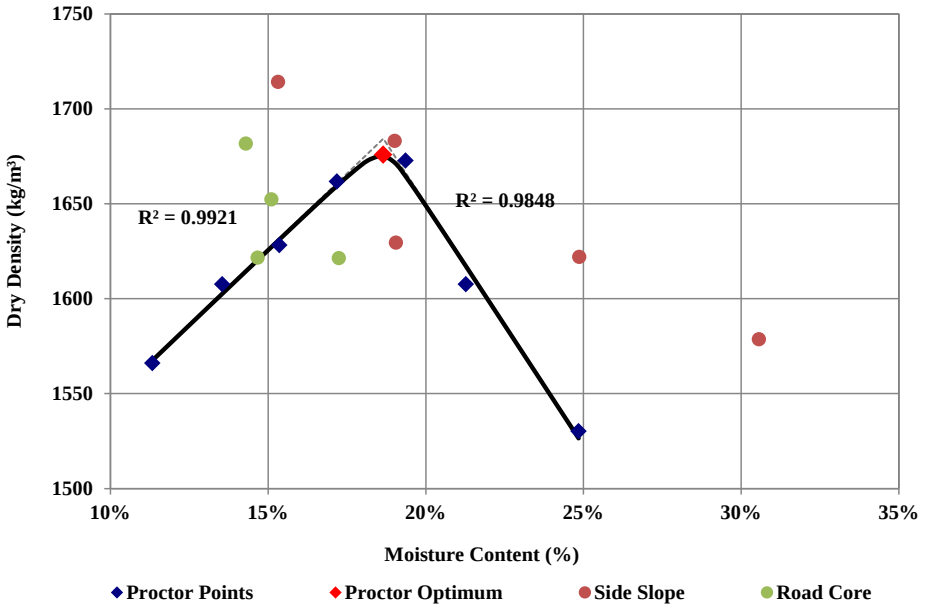

Figure 2 **Standard Proctor Characterization and *in situ* Moisture-Density - BP A**

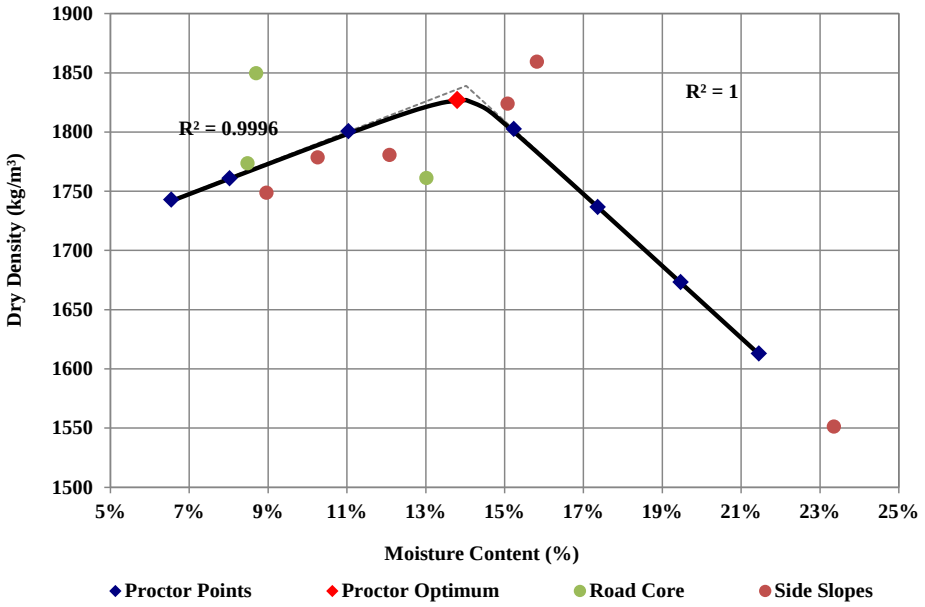

Figure 3 Standard Proctor Characterization and *in situ* Moisture-Density - BP B

MECHANISTIC MATERIALS CHARACTERIZATION

Based on the preliminary geotechnical testing, a significant range in moisture contents and densities was observed within the segments. As a result, gyratory samples were prepared and triaxial frequency sweep testing was performed on continuum samples prepared at optimum moisture and density as well as dry/low density and wet/low density conditions representative of the observed *in situ* range of each borrow material placed within the road. The mechanistic characterization was performed across stress states and load frequencies as per the specified load limits, posted traffic speed and structural layer thicknesses recommended for the particular road structure.

The subgrade materials showed considerable sensitivity in mechanical behaviour relative to *in situ* moisture content and density when subject to *in situ* field state loading conditions. This sensitivity is evident across the high variability of the non-linear dynamic modulus. Non-linear dynamic modulus was characterized across the full range of field stress states and load frequencies representative of the design field state conditions; results are provided in Table 4 below. The dynamic modulus is a measure of the stiffness of a material. All subgrade materials exhibited a decrease in dynamic modulus with increasing moisture content.

Table 4 Non-Linear Dynamic Modulus Results

Test Holes	Borrow Pit (BP)	Location (km limits)	Moisture/Density Condition	Range of Dynamic Modulus (MPa) Across Stress State and Load Frequency		
				Avg	Min	Max
1 to 8	BP A	1.4 to 2.11	Dry/Low	88	59	126
			Opt/Opt	49	31	75
			Wet/Low	10	10	10
37 to 54	BP B	2.11 to 4.9	Dry/Low	157	108	219
			Opt/Opt	98	66	140
			Wet/Low	10	10	26

Non-linear Poisson's ratio was characterized across the full range of field stress states and load frequencies representative of the design field state conditions, as seen in Table 5 below. Poisson's ratio is a ratio of the vertical to lateral strain translation, and is therefore a critical input into numerical modeling simulations. BP B dry exhibited the lowest Poisson's ratio across the subgrades characterized. All subgrade materials exhibited an increase in Poisson's ratio with increasing moisture content.

Table 5 Non-Linear Poisson's Ratio Results

Test Holes	Borrow Pit (BP)	Location (km limits)	Moisture/Density Condition	Range of Poisson's Ratio Across Stress State and Load Frequency		
				Avg	Min	Max
1 to 8	BP A	1.4 to 2.11	Dry/Low	0.30	0.26	0.36
			Opt/Opt	0.41	0.37	0.45
			Wet/Low	0.45	0.35	0.45
37 to 54	BP B	2.11 to 4.9	Dry/Low	0.20	0.12	0.27
			Opt/Opt	0.33	0.32	0.41
			Wet/Low	0.45	0.21	0.45

Non-linear phase angle was characterized across the full range of field stress states and load frequencies representative of the design field state conditions, as seen in Table 6 below. Phase angle is an indication of the viscoelastic behaviour of the materials; higher phase angles indicate that more permanent strain is occurring in a material, relative to recoverable strain for a given loading. All subgrade materials exhibited an increase in phase angle with increasing moisture content.

Table 6 Non-Linear Phase Angle Results

Test Holes	Borrow Pit (BP)	Location (km limits)	Moisture/Density Condition	Range of Phase Angle (Degrees) Across Stress State and Load Frequency		
				Avg	Min	Max
1 to 8	BP A	1.4 to 2.11	Dry/Low	12.4	5.3	17.1
			Opt/Opt	15.3	8.1	20.9
			Wet/Low	26.5	19.4	35.8
37 to 54	BP B	2.11 to 4.9	Dry/Low	11.1	5.9	15.8
			Opt/Opt	13.7	4.1	18.9
			Wet/Low	36.5	27.3	48.1

3D ROAD MODELING RESULTS

Numerical modeling was conducted using material property inputs from the mechanistic characterization of road materials and the structural design geometry specified in the road design. The 3D numerical modeling uses fully non-linear material constitutive properties, across both stress and load frequencies. Simulations of the five segments across four potential subgrade moisture-density conditions were evaluated for a B-train loaded to primary weights. Three loading conditions were evaluated: loading on the driving lane only; passing lane only; and both lanes simultaneously loaded. Driving lane results are included in this paper. The numerical modeling mesh contained over 5 million finite elements in a full three dimensional simulation of a roadway that is 50 m long and two lanes wide, with layer thicknesses and side slope geometric measurements as provided by the contractor. PSIPave3D™ utilized actual measured material properties retrieved from field samples. Results are presented at highway speeds in the driving lane, in the passing lane, and in both lanes concurrently for the five subgrade segments.

Numerical road structural modeling using field state material properties, structural cross section, and traffic loading conditions was conducted to determine the response of the road structure using standard accepted construction practices (optimum conditions) and compare this to the range in measured conditions on the roadway (Dry As Built and Wet As Built). An additional modeling case was run for each segment (Entire Subgrade Wet of Optimum) to determine the potential structural response of the segments of the roadway in the event that the structure is exposed to moisture (e.g., due to spring run-off and/or capillary rise through low density/high air void materials). This case is considered to be a worst case scenario of reasonable potential to occur in the future.

In summary, the four subgrade moisture-density conditions evaluated included:

1) Target optimum design (core/side slopes), wet deep *in situ* subgrade;
2) Dry as built condition;
3) Wet as built condition; and
4) Entire subgrade (core/side slopes/deep *in situ*) wet of optimum.

Peak Surface Deflection Profiles

Figure 4 and Figure 5 show the peak surface deflections consistently increased when comparing from target optimum design, wet deep *in situ* subgrade conditions to wet as built condition with the exception of borrow pit BP B which had a minor decrease in values. Predicted peak deflections directly related to subgrade condition, which explains the greater increases in the wet scenarios. BP B appears to have low sensitivity to moisture, which was demonstrated in the laboratory testing analysis.

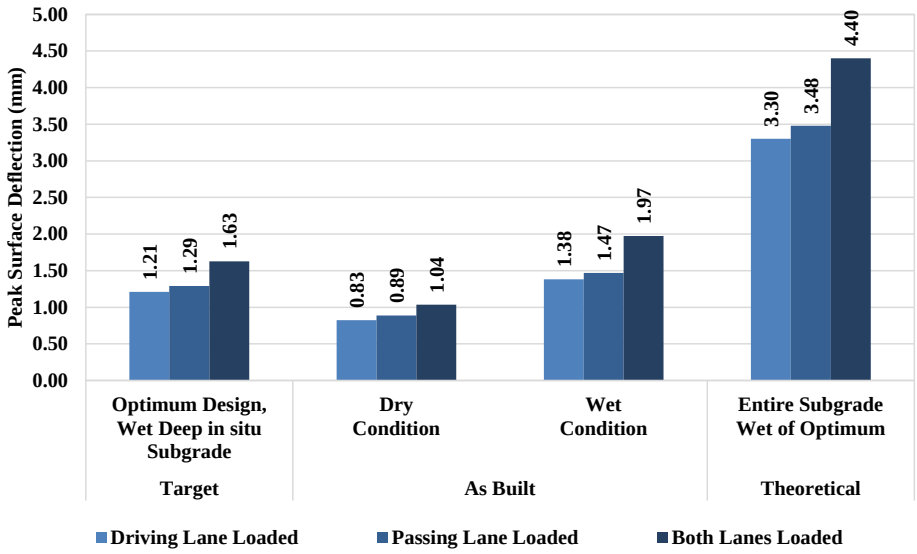

Figure 4 Peak Surface Deflection - BP A

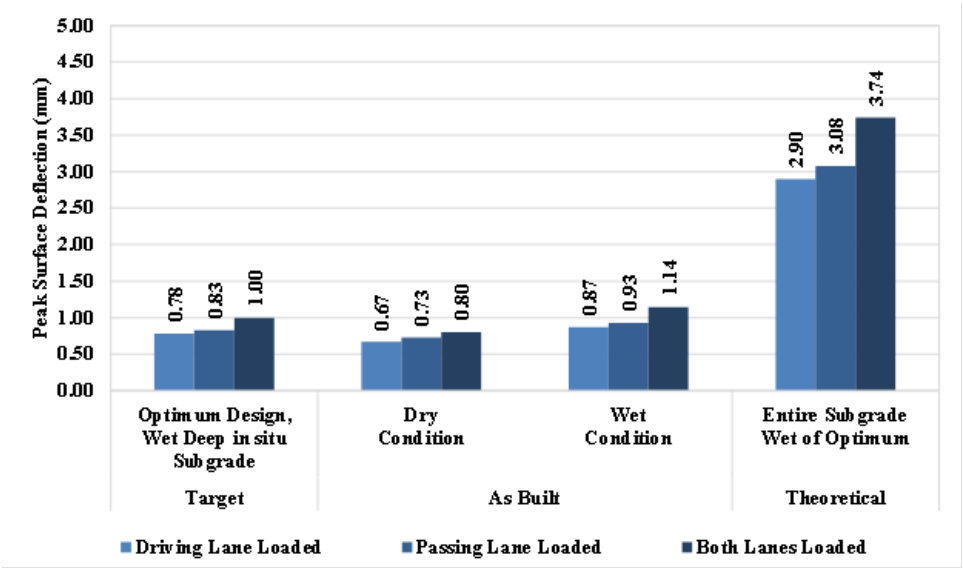

Figure 5 Peak Surface Deflection - BP B

Tensile Strain at Bottom of Asphalt Driving Lane Loading

Tensile strain at the bottom of the asphalt characterizes the rigidity of the hot mix asphalt concrete (HMAC) layer. A significant difference in stiffness in the interface between the top layer and the base layer induces a stress discontinuity and stress concentrations. In addition, a loaded thin asphalt layer tends to flex more than a loaded thicker asphalt layer. This flexing phenomenon causes the asphalt layer to flex as a beam, where high tensile strains/stresses occur at the bottom, tending to cause cracks from the bottom up.

The tensile strain does not increase in the same magnitude as the peak surface deflection when comparing the wet as built condition and the entire subgrade wet of optimum. This reduced increase can be explained by the fact that the tensile strain at the bottom of asphalt layer is predominantly a function of the load. The load is far away from the subgrade; therefore, a wet subgrade has a less significant impact on the tensile strain at the bottom of the asphalt layer. With the exception of the extreme case of the entire subgrade being wet of optimum, Figure 6 shows that the tensile strain at the bottom of the asphalt layer is relatively invariant.

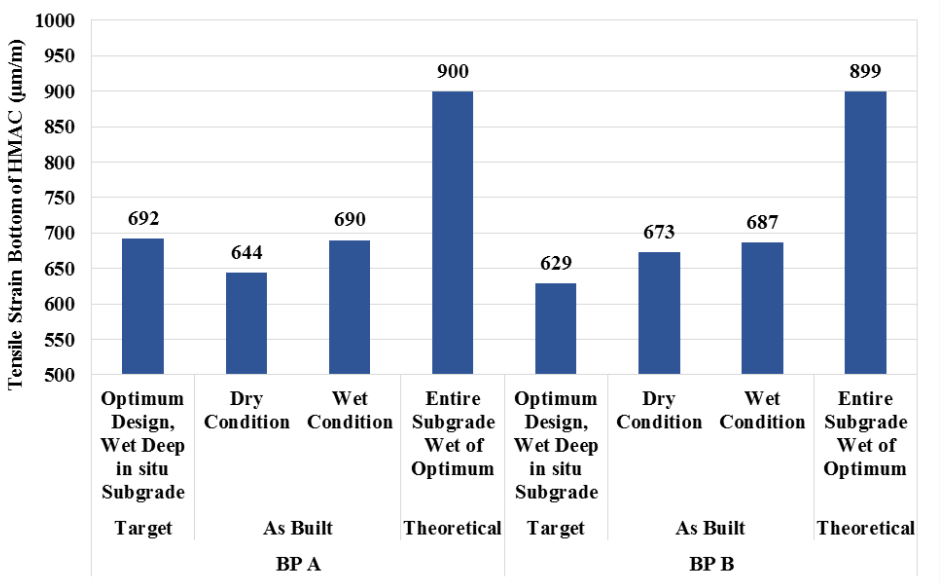

Figure 6 Tensile Strain at Bottom of Asphalt - BP A & BP B (Driving Lane Loading)

Compressive Strain at Top of Subgrade Driving Lane Loading

Compressive strain at the bottom of the subgrade relates directly to the competence of the pavement structure on top of it. High compressive strains at the bottom of the subgrade signify the applied loads are not being dissipated by the structural layers. Therefore, high compressive strains induced in the weakest material (the subgrade) are related to rutting at the surface. As the subgrade gets compressed, the entire structural layers also get compressed, causing rutting. A wet subgrade, as seen in the results from Figure 7 below, has a significant impact on compressive strains at the bottom subgrade.

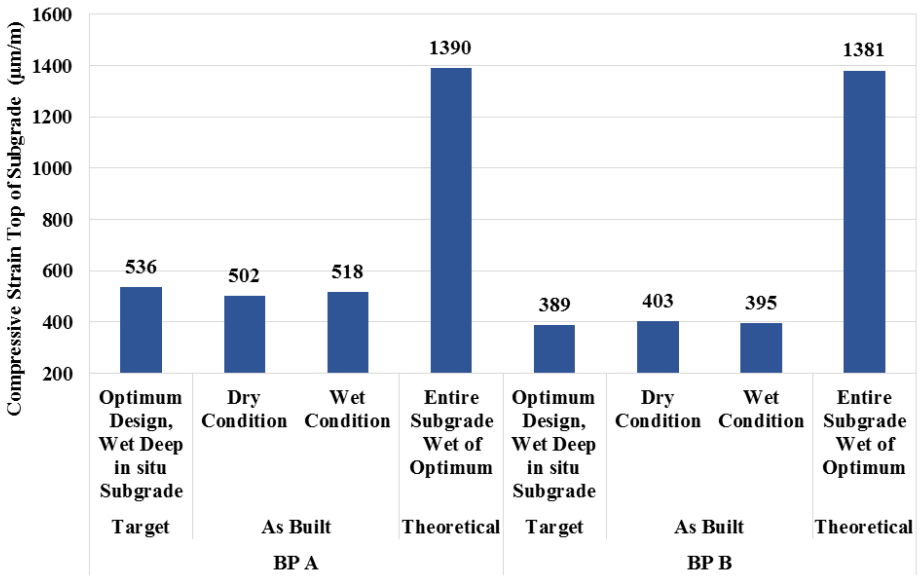

Figure 7 Compressive Strain at Top of Subgrade - BP A & BP B (Driving Lane Loading)

Peak Shear Strain Driving Lane Loading

Failure in pavements commonly occurs due to high shear strains concentration. Accurate prediction of the peak shear strains in a pavement structure is important in determining how/if the pavement will fail. However, the percentage increases and/or decreases follow a different pattern than the orthogonal components of strain. Shear strains are directly related to dislocation of planes with respect to each other. When a wheel load passes on a road asphalt surface, shear stresses occur in the asphalt layer. The shear stresses induce sliding between the edge of the tires and the pavement, both at high and low travelling speeds. If an asphalt layer is cracked, the shear stresses in the asphalt layer can propagate through the crack and into the base layer or other pavement layers of the road structure. Therefore, quantifying shear strains is vital to a haul road both higher speeds as well as in low speed, which occur when trucks slow down and turn. In wet conditions, roads can fail in shear with just one overloaded truck. Peak shear strains in each pavement layer are identified in Figure 8 and Figure 9 below.

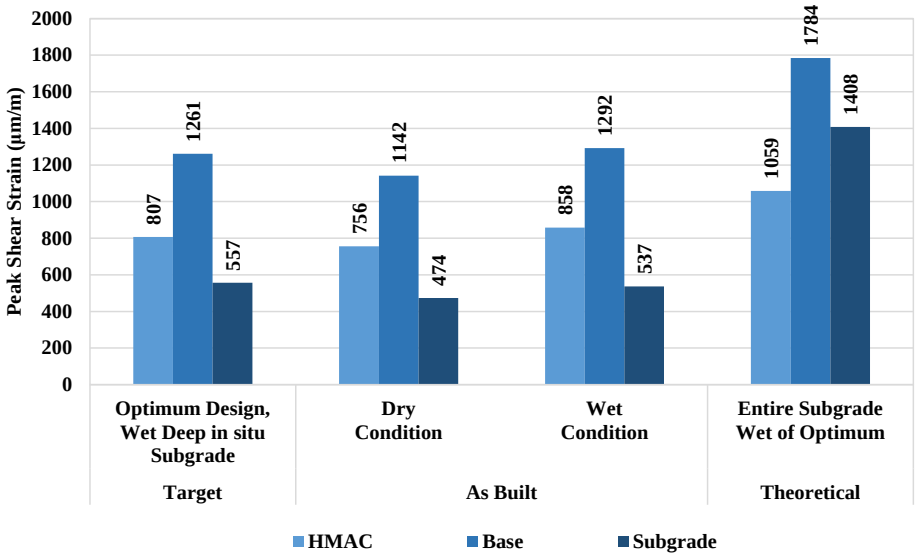

Figure 8 Peak Shear Strain - BP A (Driving Lane Loading)

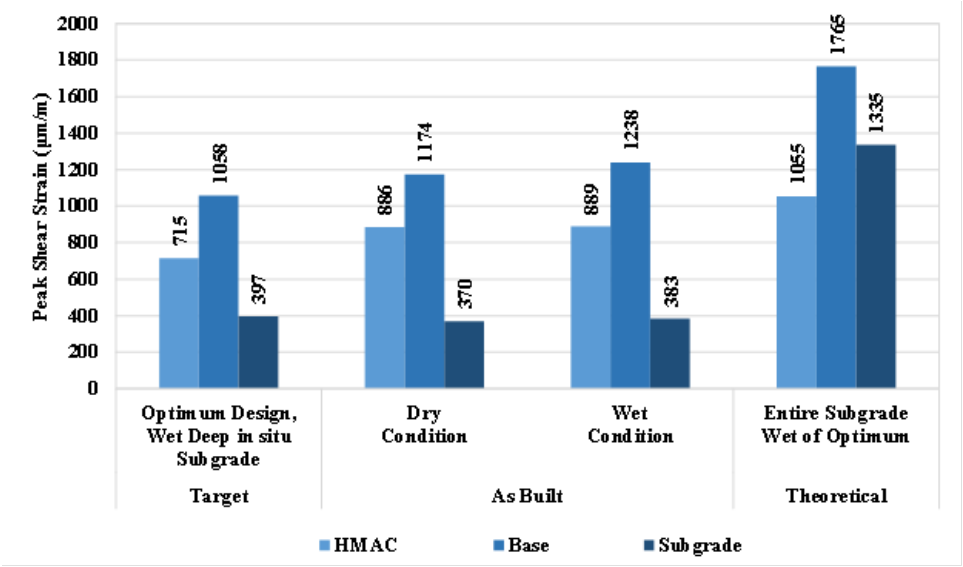

Figure 9 Peak Shear Strain - BP B (Driving Lane Loading)

Note that Figure 8 presents higher peak shear strain values than Figure 9, demonstrating the improved quality of BP B materials. The base layer has the highest peak shear of all three layers, which indicates it is taking some of the load being dissipated by the HMAC. The HMAC is the stiffer, more resistant material; therefore it can sustain higher levels of strain. The subgrade is the weakest and can only take a small amount of strain. Figure 10 and Figure 11 illustrate a cross section cut on longitudinal and transversal directions of the entire pavement. The figures shows shear contour through depth into the pavement layers (red illustrates high shear strain levels). It can be seen by both Figure 10 and Figure 11 that subgrade shears are smaller compared to the base (base is located at the upper portion compared to subgrade at the lower portion), illustrating proper shear strain dissipation through the layers.

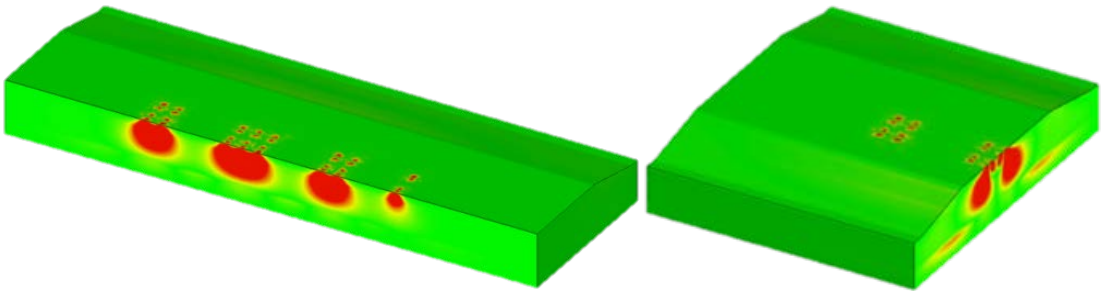

a) Target Optimum Design (Core/Side Slopes), Wet Deep *In Situ* Subgrade

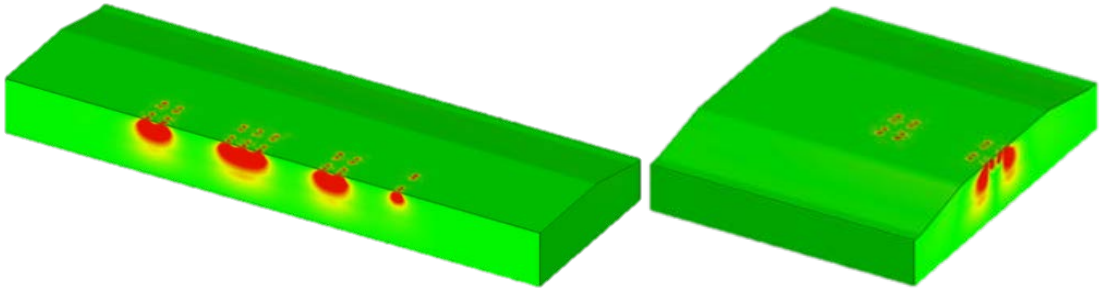

b) Dry As Built Condition

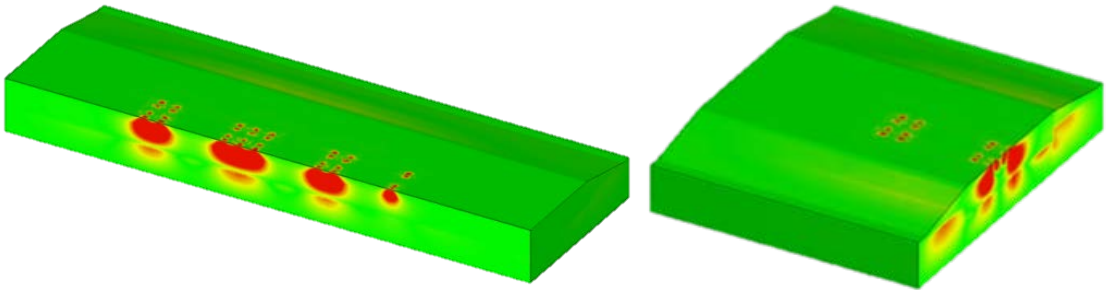

c) Wet As Built Condition

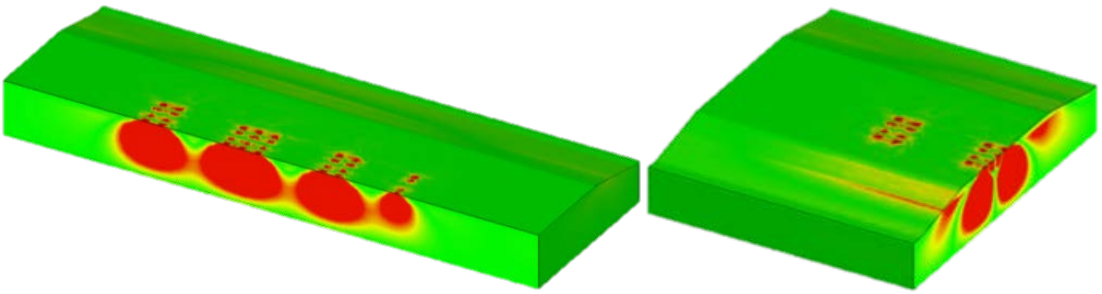

d) Entire Subgrade (Core/Side Slopes/ Deep *In Situ*) Wet of Optimum

Figure 10 Shear Strain Profile Across Road Length and Width BP A (Driving Lane Loading)

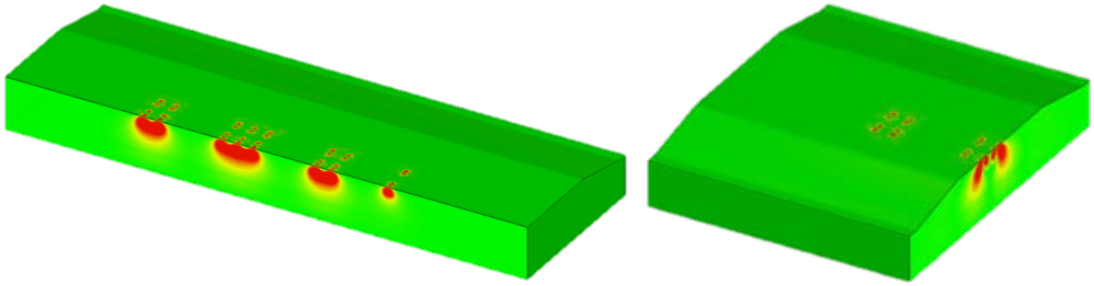

a) Target Optimum Design (Core/Side Slopes), Wet Deep *In Situ* Subgrade

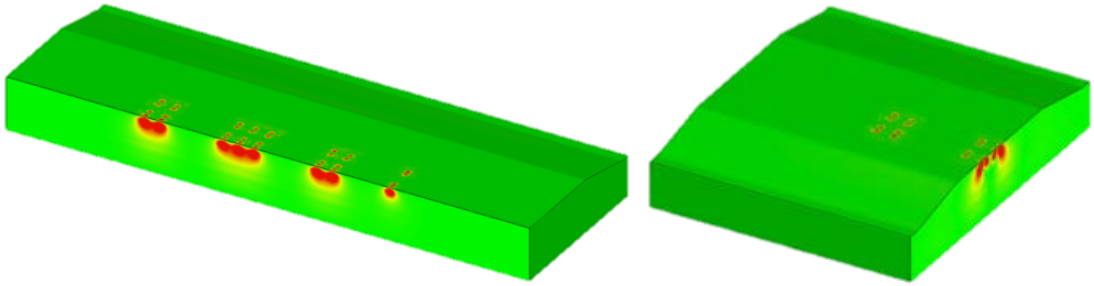

b) Dry As Built Condition

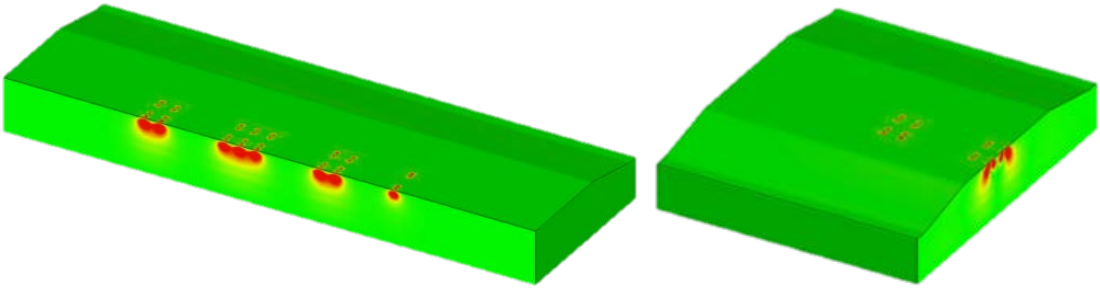

c) Wet As Built Condition

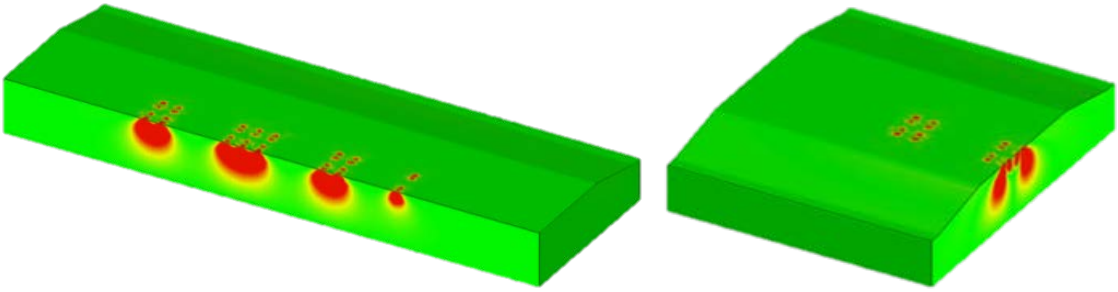

d) Entire Subgrade (Core/Side Slopes/Deep *In Situ*) Wet of Optimum

Figure 11 Shear Strain Profile Across Road Length and Width – BP B (Driving Lane Loading)

CONCLUSION

The finite element model characterized the effect of the *in situ* variability under typical truck loading specified for the analyzed heavy haul road in Western Canada as well as expected future climatic conditions typical of the area. The results of the modelling investigation showed significant variation in peak surface deflection, volumetric deflection, tensile and compressive strain profiles. Based on the numerical modeling with PSIPave3D™ that was conducted herein using material property inputs from the mechanistic characterization and the structural design geometry specified for the service road, the following was observed:

- All segments exhibited good structural response under dry as built conditions, indicating that the target optimum design was achieved in localized areas within each segment.
- Variability of moisture and density was high within BP A which results in the varied structural response within these segments from the dry as built to wet as built conditions.
- BP B exhibited good structural response under both dry as built and wet as built conditions.
- Materials from BP A exhibited potential to rapidly degrade if exposed to higher moisture conditions, therefore a potential for structural weakening exists.

Based on the primary response profiles of the various road segments modelled under realistic Canadian field state conditions, the *in situ* variability is expected to have highly variable life cycle structural performance.

References

1) AASHTO. Guide for Mechanistic-Empirical Design of New and Rehabilitated Structures. Washington, D.C., 2002.
2) Classed, A., Edwards, J., Sommer, P., and P. Uge. Asphalt Pavement Design – The Shell Method. 4th International Conference, Structural Design of Asphalt Pavements. Ann Arbor, Michigan, 1977, pp.39-74.
3) Al-Qadi, I.L., Wang, H., Peong, J.Y., and Dessouky, S.H. 2008. Dynamic Analysis and In Situ Validation of Perpetual Pavement Response to vehicular Loading. Transportation Research Record: Journal of the Transportation Research Board No. 2087. Transportation Board of the National Academies, Washington, D.C., pp.29-39. DOI: 10.3141/2087-04
4) Guenther, D., Haichert, R., Soares, R., and Berthelot, C. 2013. Mechanistic Design: A Modeling Case Study for the City of Saskatoon. Transportation Association of Canada (TAC) Annual Conference, Winnipeg, MB.
5) Prang, C., Podborochynski, D., Kelln, R., Berthelot, C. 2012. City of Saskatoon's Pavement Management System: Network Level Structural Evaluation. Submitted to Journal of the Transportation Research Board of the National Academies, TRB 91sth Annual Meeting, January 22-26, 2012, Washington, D.C. USA. (Paper #12-1369)
6) Berthelot, C., Soares, R., Haichert, R., Podborochynski, D., Guenther, D., Kelln, R. 2012. Modeling the Performance of Urban Structural Sub-Surface Drainage Systems. Transportation Research Record: Journal of the Transportation Research Board of the National Academies, Washington, D.C. USA. Vol. 2282. p.p.34-42.
7) Allen, D., Little, D., Soares, R., Berthelot, C. 2015. "Multi-Scale Computational Model for Design of Flexible Pavement – Part III: Two-Way Coupled Multi-Scaling", International Journal of Pavement Engineering.
8) Allen, D., Little, D., Soares, R., Berthelot, C. 2015. "Multi-Scale Computational Model for Design of Flexible Pavement – Part II: Contracting Multi-Scaling", International Journal of Pavement Engineering.
9) Allen, D., Little, D., Soares, R., Berthelot, C. 2015. "Multi-Scale Computational Model for Design of Flexible Pavement – Part I: Expanding Multi-Scaling", International Journal of Pavement Engineering.